Optimization of sulfate removal from brackish water by membrane capacitive deionization (MCDI)

Wangwang Tang, Di He[**], Changyong Zhang, T. David Waite[*]

School of Civil and Environmental Engineering, University of New South Wales, Sydney, NSW 2052, Australia

ABSTRACT

Removal of sulfate from water is an environmental challenge faced by many industrial sectors as most existing options are inefficient, costly or unsustainable. The situation is further complicated by the typical coexistence of other ions. In this work, the feasibility of sulfate removal from brackish water by single-pass constant-current membrane capacitive deionization (MCDI) under reverse-current desorption was investigated. Results revealed that sulfate is preferentially removed from the aqueous solution by MCDI compared to chloride. Equivalent circuits of the MCDI system during adsorption and desorption were proposed and the dynamic variation of cell voltage and charging voltage at different adsorption currents was satisfactorily elucidated. Optimization studies were conducted with attention given to discussing the effects of four operating parameters, i.e., adsorption current, pump flow rate, ending cell voltage and desorption current, on three performance indicators (i.e., water recovery, energy consumption and sorption ratio of sulfate to chloride) on the premise of maintaining the effluent sulfate concentration below the specified threshold of 300 mg L^{-1}. Water recovery-energy consumption mapping and sorption ratio of sulfate to chloride-energy consumption mapping indicated that the combination of a lower adsorption current and a lower matching pump flow rate which reduced the effluent sulfate concentration to 300 mg L^{-1} was more favorable in practical applications. An appropriately small ending cell voltage was advantageous while a trade-off between water recovery and energy cost was required in optimizing the desorption current.

© 2017 Elsevier Ltd. All rights reserved.

1. Introduction

Sulfate (SO_4^{2-}) is ubiquitous not only in natural waters, but also in municipal and industrial wastewaters (Călinescu et al., 2016; Runtti et al., 2016). Although sulfate is not usually considered a health concern, high concentrations of sulfate in drinking water can cause a bitter taste and, when its concentration exceeds 600 mg L^{-1}, diarrhea (Guimarães and Leão, 2014). Discharge of high levels of sulfate can significantly affect public water supplies by causing corrosion and/or scaling of pipes and equipment. Moreover, hydrogen sulfide (H_2S), which is toxic to the ecosystem, could be produced through sulfate reduction by sulfate-reducing bacteria under anaerobic conditions (Chen et al., 2016). Because of these adverse effects to human health and the environment, many countries have set the maximum sulfate concentration values

ranging from 250 mg L^{-1} to 500 mg L^{-1} depending on the end use of the water source (Runtti et al., 2016). In addition, it is important to remove sulfate from recycled wastewater when transferring the concentrate from the membrane separation process back to the initial biological system (such as a membrane bioreactor) in order to minimize the effects of sulfate on both the efficacy of the biological process and membrane scale formation. To date, several methods have been applied in treating waters containing excessive sulfate, including chemical precipitation, adsorption and/or ion exchange, biological treatment and reverse osmosis. However, these methods suffer from limitations. For example, precipitation and adsorption methods produce large amounts of potentially toxic sludges. Biological methods require significant amounts of organic carbon (as bacterial feed) and careful anaerobic sludge management (Silva et al., 2012). Reverse osmosis methods are costly despite enabling treatment of large volumes of waters. As such, seeking a more cost-effective, sustainable and easy-to-operate alternative method for sulfate removal is of considerable importance.

Capacitive deionization (CDI), as a cost effective, energy efficient and environmentally friendly electrochemical technology, is attracting increasing attention for the facile removal of ionic species from water (Cohen et al., 2015; Gao et al., 2015a; Garcia-Quismondo et al., 2016; Kang et al., 2016; Suss et al., 2015; Tang et al., 2016). CDI enables ion removal at low pressures and low voltages, and has the potential to be powered by solar energy in remote areas with the additional possibility of energy recovery via the capacitive effect created on ion sorption within electrode double layers. Also, CDI operates without the use of any added chemicals or the generation of hazardous substances, with the added possibility of recovery of certain ions from the concentrate stream via precipitation of high value minerals. Generally, a CDI cell consists of two graphite current collectors facilitating electron transfer, two porous carbon electrodes for ion sorption and a spacer channel enabling water to be transported from the perimeter to the center of the unit (Porada et al., 2013). One relatively recent significant improvement in CDI is the inclusion of ion exchange membranes (IEMs) in front of the electrodes in a process known as membrane capacitive deionization (MCDI). More specifically, a cation exchange membrane is placed in front of the cathode while an anion exchange membrane is placed in front of the anode, allowing for counterion transport from the spacer channel into the electrode while preventing co-ions from leaving the electrode region. In this approach, the macropores within the electrodes serve as extra storage space for ions, thereby improving the ion removal performance (Biesheuvel et al., 2011; Choi, 2014; Porada et al., 2013). To date, most (M)CDI laboratory-scale studies have focused on applying a constant charging voltage between the electrodes during adsorption, followed by short-circuiting or reversing the voltage to regenerate the electrodes during desorption (Bian et al., 2015; Gao et al., 2015b; Mossad and Zou, 2012, 2013). However, in practical applications, constant voltage charging may be not appropriate considering that the effluent ion concentrations vary greatly with time. To obtain purified water with relatively constant ion concentrations below a specified threshold value, applying a constant current across the electrodes during charging is strongly preferred.

To compare and optimize the efficacy of (M)CDI systems, various performance indicators have been employed (Huyskens et al., 2013; Mossad and Zou, 2012; Suss et al., 2015; Zhao et al., 2013), including ion removal efficiency, effluent ion concentrations, water recovery, charge efficiency, average salt adsorption rate (ASAR) and energy consumption. The continuing rapid growth of CDI research necessitates a standardization of key performance indicators for particular applications as some indicators may be inappropriate. For example, ion removal efficiency is mainly used in batch-mode CDI tests describing the relative decrease in salt concentration in the recycled solution (Suss et al., 2015), making it unsuitable for other CDI operational modes. With the values of energy consumption known, charge efficiency appears unimportant as charge efficiency and energy consumption are closely related.

In this study, we investigate the feasibility of sulfate removal by single-pass constant-current MCDI in the presence of chloride as is typical in practical scenarios. Insights into understanding of the effects of particular operational parameters (in particular, adsorption/desorption current, pump flow rate and ending cell voltage) on system performance are provided. On the premise of maintaining the effluent sulfate concentration below 300 mg L^{-1}, two key performance indicators (i.e., water recovery and energy consumption) are used to evaluate the performance with regard to sulfate removal. The correlation between operational parameters and performance indicators is developed as a guide for optimization of MCDI operation. The preferential adsorption between sulfate and chloride as affected by the selected operational parameters is also examined.

2. Experimental

2.1. MCDI module

The MCDI module used in this study (Model No. VS1) was directly purchased from Voltea B.V. (the Netherlands) and contains a stack of 50 cells connected in parallel electrically and with regard to fluid flow. Each cell consists of two graphite sheets as current collectors which are alternatingly positively and negatively biased, two porous carbon electrodes with anion or cation exchange membranes attached to the electrode surfaces and a 200 μm thick non-conductive nylon cloth as the spacer channel. The carbon electrode is 200 cm^2 in area and 150 μm in thickness. As the MCDI module is commercially acquired, only limited information regarding the exact design and manufacturing detail of the electrode/membrane system is available. The water is pumped into the CDI module through an opening located in one of the four corners with treated water flowing out from an opening in the center of the electrode unit.

2.2. Experimental methods

The schematic diagram of the experimental setup is shown in Fig. S1. The system consists of a feed vessel, a peristaltic pump (Masterflex, Cole-Parmer, USA), a MCDI module and a DC power supply (WEP, Yihua Electronic Equipment Co., Ltd, China). In this study, although convenient, dead volume was not used for measurement of pH and conductivity due to the great difference between the measured effluent ion concentration with dead volume and that without dead volume (further details are provided in Section S2). Prior to the test, the electrical charge remaining on the carbon electrodes should be zero. Analytical grade sodium sulfate (Na$_2$SO$_4$) and sodium chloride (NaCl) were used for the preparation of feed water. All reagent solutions were prepared using 18 MΩ cm resistivity Milli-Q water unless stated otherwise. Initially, the MCDI module was fully flushed using the feed water until the effluent conductivity was close to the influent conductivity. During adsorption, a constant electrical current was applied to the module. Once the cell voltage reached a specified value, the cell was switched from adsorption to desorption mode. During desorption, we employed a constant reverse electrical current (reverse-current desorption) until the cell voltage dropped back to 0 V. The reason why reverse-current desorption instead of zero-volt desorption was used here is discussed in detail in Section S2. The cell voltage was measured using an on-line voltage probe (VP-BTA, Vernier Corp., USA) while the voltage readings of the power supply represent the charging voltage. The data were not collected until the MCDI module had been operated for a number of cycles. Water samples were taken from the outlet of the MCDI module at appropriate intervals and the effluent ion concentrations determined using an ICS-3000 ion chromatograph (Dionex, USA). Duplicate runs were carried out for each set of experimental conditions and the average value presented.

In these experiments, the water recovery was calculated as follows,

$$\text{Water recovery} = \frac{V_p}{V_T} = \frac{v_{ads} \cdot t_{ads}}{v_{ads} \cdot t_{ads} + v_{des} \cdot t_{des}} = \frac{t_{ads}}{t_{cycle}} \quad (1)$$

where V_p and V_T (m^3) are the purified water volume and total water volume produced in one cycle, respectively. v_{ads} and v_{des} (m^3 s^{-1}) are the pump flow rate during adsorption and desorption, respectively. t_{ads} (s) is the adsorption time, t_{des} (s) is the desorption time and t_{cycle} (s) is the sum of t_{ads} and t_{des}. In our study, as v_{ads} was equal to v_{des}, a simplified expression for water recovery can be expressed

as t_{ads}/t_{cycle}.

The electrical energy consumption W (kJ m^{-3} purified water produced) was calculated according to,

$$W = \left(I_{ads} \cdot \int_{t_0}^{t_{ads}} V_{ch} \cdot dt + I_{des} \cdot \int_{t_{ads}}^{t_{cycle}} V_{ch} \cdot dt \right) \times 10^{-3} \Big/ V_p \qquad (2)$$

where I_{ads} and I_{des} (A) represent the adsorption current and the desorption current, respectively. V_{ch} (V) represents the charging voltage.

The specific ion j adsorption per cycle, Γ_j (mol), is derived by integrating the difference between the feed concentration $c_{j,feed}$ (mM) and the effluent concentration $c_{j,eff}$ (mM) over time ($t_0 \rightarrow t_{ads}$) and multiplying by the pump flow rate v_{ads}. The mathematical expression for the specific ion adsorption per cycle can be written as

$$\Gamma_j = v_{ads} \int_{t_0}^{t_{ads}} \left(c_{j,feed} - c_{j,eff} \right) dt \qquad (3)$$

3. Results and discussion

3.1. Differential separation between sulfate and chloride

To explore the differential separation between sulfate and chloride in the MCDI cells, 15 mM Na$_2$SO$_4$ and 15 mM NaCl were used as the feed water under the operating conditions of adsorption current 2 A, desorption current −3 A (where "minus" represents polarity reversal), pump flow rate 50 mL min^{-1} and ending cell voltage 1.2 V. Fig. 1 shows the profiles of effluent SO$_4^{2-}$ and Cl$^-$ concentrations within a full cycle. As can be seen, SO$_4^{2-}$ and Cl$^-$ display similar adsorption and desorption behaviors, i.e., after the commencement of the adsorption, the effluent SO$_4^{2-}$ and Cl$^-$ concentrations decrease quickly and then level off, followed by a rapid increase and attainment of an almost constant concentration during desorption. Moreover, it is found that the effluent SO$_4^{2-}$
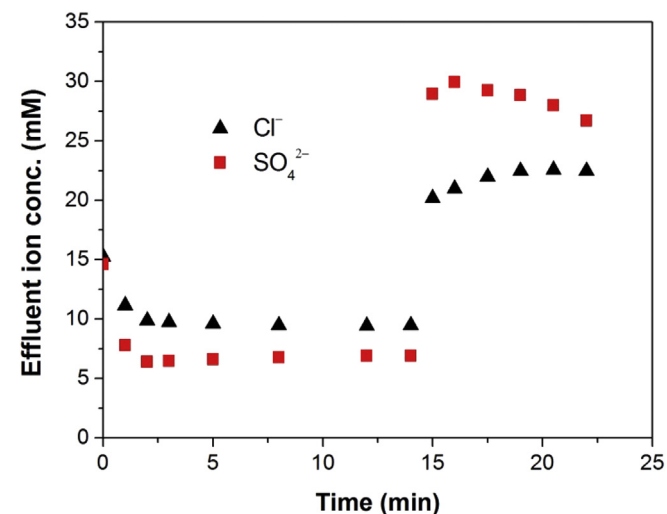

Fig. 1. Differential separation between sulfate and chloride in MCDI cells. Experimental conditions: sulfate feed concentration 15 mM, chloride feed concentration 15 mM, adsorption current 2 A, desorption current −3 A, pump flow rate 50 mL min^{-1} and ending cell voltage 1.2 V.

concentration remains consistently below and above the effluent Cl$^-$ concentration during adsorption and desorption, respectively, which suggests that SO$_4^{2-}$ is preferentially removed from the aqueous solution passing through the spacer channels in the MCDI cells. The preferential adsorption of SO$_4^{2-}$ over Cl$^-$ can be explained from the Nernst-Planck equation describing the flux of ions approaching the electrode (Tang et al., 2015), $J_j = -D_j \cdot (dc_j/dX + z_j \cdot c_j \cdot d\phi/dX)$, where J_j is the flux of ion j (mol m^{-2} s^{-1}), D_j is the diffusion coefficient of ion j (m^2 s^{-1}) ($D_{SO4} = 1.07 \times 10^{-9}$, $D_{Cl} = 2.03 \times 10^{-9}$ m^2 s^{-1}) (Flury and Gimmi, 2002), c_j is the concentration of ion j (mM) in the spacer channel and z_j is the ion charge number. Under the assumptions of gradientless concentration profile and a linearized potential profile, the flux ratio of SO$_4^{2-}$ to Cl$^-$ is simplified to $D_{SO_4} \cdot z_{SO_4} \cdot c_{SO_4}/(D_{Cl} \cdot z_{Cl} \cdot c_{Cl})$, which can be further simplified to $D_{SO_4} \cdot z_{SO_4}/(D_{Cl} \cdot z_{Cl})$ under the conditions of equal initial concentrations of SO$_4^{2-}$ and Cl$^-$ in the spacer channel. The value of $D_{SO_4} \cdot z_{SO_4}/(D_{Cl} \cdot z_{Cl})$ is calculated to be greater than 1, suggesting that, compared to Cl$^-$, more SO$_4^{2-}$ is subject to transport from the spacer channel to the anode in a certain period of time with higher adsorption capacity in terms of SO$_4^{2-}$. While the dual anion cases may be at the simpler end of natural water conditions, the mathematical approach shown here could potentially be used to qualitatively assess the preferential ion adsorption in (M)CDI for real waters (e.g., brackish groundwater) where multiple anions or cations are present at varying concentrations.

3.2. Characterization of electric circuit of the MCDI system

The variation of cell voltages during adsorption was investigated at different adsorption currents with the results obtained shown in Fig. 2a. From these results it can be observed that the cell voltage increased rapidly at the initial stage after the adsorption current was applied and then gradually increased linearly. Meanwhile, an increase in adsorption current led to a linear increase in the initial cell voltage along with a decrease in the time required to reach the final cell voltage. The charging voltages during adsorption at different adsorption currents were also recorded and it was found that the difference between the charging voltage and the cell voltage increased in direct proportion to the increase of the adsorption current (Fig. S4), implying that the external electrical resistance (R_{ext}) in the MCDI system was constant.

A simple model was proposed to characterize the electric circuit of the MCDI system during adsorption and desorption as displayed in Fig. 2c and d. By ignoring the electrical resistance and contact interfacial resistance of current collectors and carbon electrodes (Qu et al., 2015), the MCDI cell can be simply considered to consist of two electric double layer (EDL) capacitors and resistances of the ion exchange membranes and the spacer electrolyte solution. Before supplying adsorption current to the MCDI cells, the carbon electrodes were not charged. At the moment of connecting the circuit, the voltage across the two EDL capacitors is zero and the voltage across the ion exchange membranes and the spacer electrolyte solution represents the cell voltage. As a result, the initial electrical resistance of the cells was calculated to be 0.099 Ω according to the relationship between initial cell voltage and adsorption current as indicated by the inset in Fig. 2a. The resistances of the ion exchange membranes and the spacer electrolyte solution are inversely proportional to the ion concentrations in the spacer (Biesheuvel et al., 2011; Dykstra et al., 2016), which can be simply expressed as d/κ (where d is the spacer thickness and κ is the electrical conductivity of the spacer solution) (Crow, 1994). With this formula, the cell voltage (U_{cell}) during adsorption is further given by
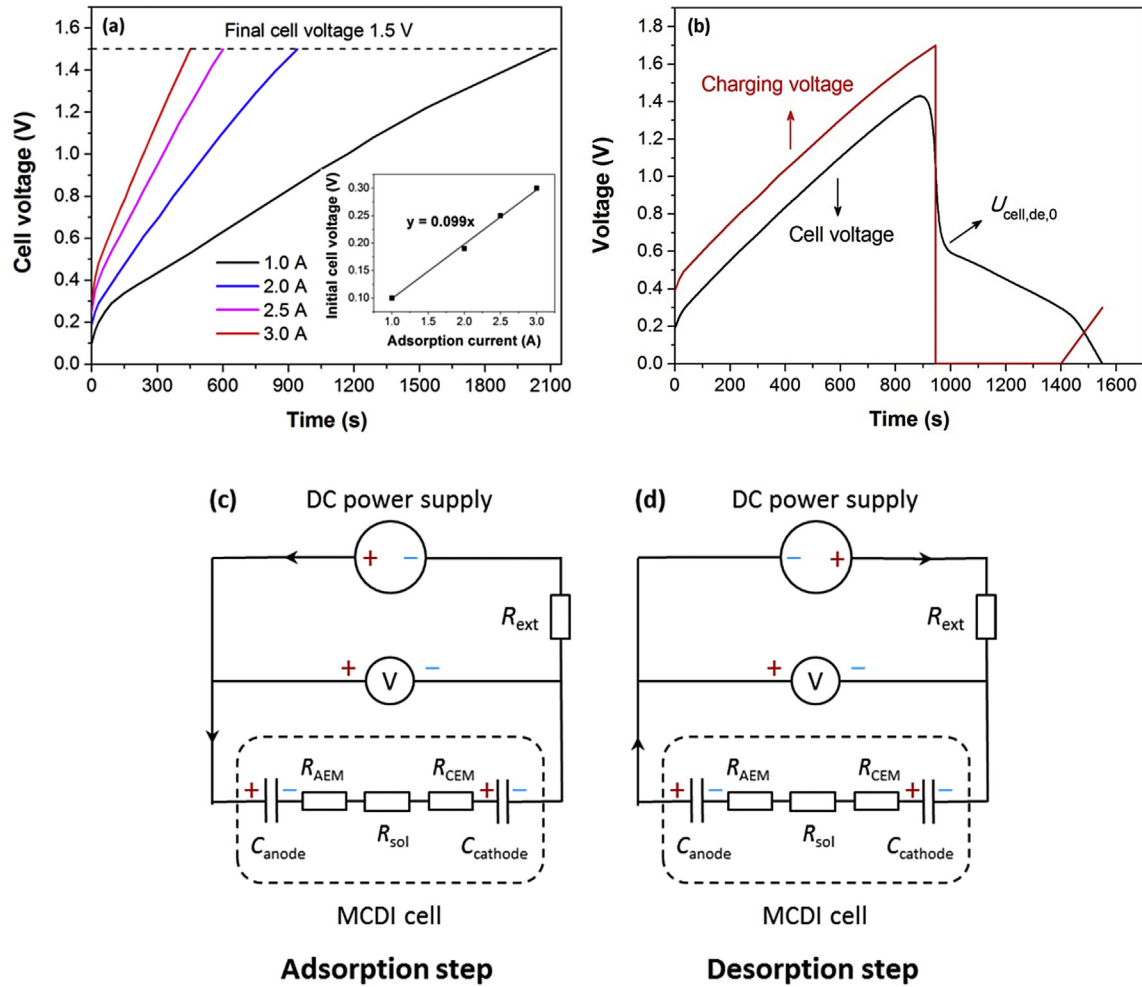
Fig. 2. **(a)** The measured cell voltages during adsorption at different adsorption currents. The inset indicates the initial cell voltage versus the adsorption current. Experimental conditions: sulfate feed concentration 1000 mg L^{-1}, chloride feed concentration 500 mg L^{-1} and pump flow rate 50 mL min^{-1}; **(b)** Dynamic variation of cell voltage and charging voltage during adsorption and desorption. Experimental conditions: sulfate feed concentration 1000 mg L^{-1}, chloride feed concentration 500 mg L^{-1}, adsorption current 2 A, pump flow rate 50 mL min^{-1}, ending cell voltage 1.5 V and desorption current −3 A; **(c, d)** Equivalent circuit of the MCDI system during adsorption and desorption. R_{ext}, R_{sol}, R_{AEM}, R_{CEM} represent the external electrical resistance, resistance of the solution in the spacer channel, resistance of the anion exchange membrane and resistance of the cation exchange membrane, respectively. C_{anode} and $C_{cathode}$ represent the electric double layer capacitance of the anode and cathode, respectively.

$$U_{cell} = I_{ads} \cdot d/\kappa + 2I_{ads} \cdot t/C \qquad (4)$$

where C denotes the EDL capacitance of the anode or cathode. Derivatizing Eq. (4) yields

$$\frac{dU_{cell}}{dt} = -\frac{I_{ads} \cdot d}{\kappa^2} \cdot \frac{d\kappa}{dt} + 2 \cdot \frac{I_{ads}}{C} \qquad (5)$$

where $d\kappa/dt$ represents the rate of change in electrical conductivity of the spacer solution over time. After an adsorption current is supplied to the MCDI cells, ions are adsorbed and the value of κ decreases and $d\kappa/dt$ becomes negative with its absolute value decreasing until it approaches zero when the ion concentrations in the spacer become stable. Accordingly, dU_{cell}/dt decreases and then remains constant when $d\kappa/dt$ is equal to zero, which, up to this point, provides a satisfactory interpretation of the dynamic variation in cell voltage during adsorption as shown in Fig. 2a. As for the external electrical resistance (R_{ext}) of the MCDI system, it was determined to be 0.1 Ω based on the profile of the difference between the charging voltage and the cell voltage versus the adsorption current during adsorption (see Fig. S4).

In addition to enabling us to elucidate the dynamic variation of cell voltage and charging voltage at different adsorption currents during adsorption, the characterization of the electric circuit of the MCDI system can also be used to explain the substantial difference between the cell voltage and the charging voltage during desorption (Fig. 2b). Assuming that, at the moment of switching from adsorption to desorption, the resistances of the ion exchange membranes and the spacer electrolyte solution under the experimental conditions of Fig. 2b were R (Ω), and the voltage across the two EDL capacitors was U (V), then, the following equations are satisfied according to Kirchhoff's law:

At the end of adsorption : $U + I_{ads}(R + R_{ext}) - U_{ch} = 0$ (6)

At the start of desorption : $-U + I_{des}R + U_{cell,de,0} = 0$ (7)

where I_{ads} and I_{des} represent the adsorption current (2 A) and desorption current (3 A), respectively. U_{ch} represents the charging voltage at the end of adsorption (1.7 V). $U_{cell,de,0}$ (V) represents the

cell voltage at the start of desorption (0.625 V) which can be obtained from Fig. 2b. Substituting I_{ads}, I_{des}, R_{ext}, U_{ch} and $U_{cell,de,0}$ into Eqs. (6) and (7), we obtain $U = 1.15$ V, $R = 0.175$ Ω. The value of R is quite reasonable considering that the initial resistances of the ion exchange membranes and the spacer electrolyte solution were 0.099 Ω and noting that R should be larger than 0.099 Ω in achieving the steady-state ion concentrations in the spacer. On reversing the DC power polarity, the two EDL capacitors would be expected to act as a power source with charge neutralization of the capacitors leading to a gradual decrease in the cell voltage. As shown in Fig. 2b, this predicted behavior is consistent with the results obtained. In addition, the voltage across the DC power supply at the beginning of desorption is calculated to be $-U_{cell,de,0} + I_{des}R_{ext} = -0.325$ V, implying that the DC power supply becomes an electric load component instead of a constant current power source. Indeed, this is the reason why the charging voltage drops to 0 V until the voltage across the DC power supply reaches a positive value.

It should be noted that the ion adsorption capacity of the carbon electrodes depends on the voltage across the two EDL capacitors rather than the cell voltage, whereas the energy consumption is closely related to the charging voltage. In providing a good description of the obtained voltage data, the simple circuit model proposed here also suggests that an increase in the capacitance of carbon material is beneficial to enhancing the ion adsorption capacity by consuming the same amount of electrical energy while a decrease in the external electrical resistance and/or the resistances of the ion exchange membranes and the spacer electrolyte solution is conducive to reducing the energy consumption by adsorbing the same number of ions.

3.3. Optimization of operating parameters

For the single-pass constant-current MCDI tests under reverse-current desorption, generally, the desalination performance depends strongly on four operating parameters when the influent ion concentrations are fixed, namely, adsorption current, water flow rate, ending cell voltage and desorption current. In this section, optimization of sulfate removal in the presence of chloride using MCDI is addressed by examining the effects of the four operating parameters on the two key performance indicators, i.e., water recovery and energy consumption, on the premise that the effluent sulfate concentration is maintained below the specified threshold of 300 mg L^{-1}.

It has been reported that the effluent ion concentration could be adjusted to a certain set point only by either varying the adsorption current and/or the water flow rate for particular (M)CDI configurations and source waters of particular composition (Zhao et al., 2013). In preliminary studies, we found that, for a given feed solution of 1000 mg L^{-1} sulfate and 500 mg L^{-1} chloride, 2 A adsorption current and 50 mL min^{-1} pump flow rate could reduce the effluent sulfate concentration to about 300 mg L^{-1}. Figs. 3 and 4 show the effects of adsorption current and pump flow rate, respectively, on the effluent sulfate and chloride concentrations with the results indicating that a larger adsorption current or a lower pump flow rate contributes to decreasing effluent ion concentrations during adsorption. Despite the fact that desirable lower effluent sulfate and chloride concentrations were achieved under these circumstances, lower water recovery and higher energy consumption were observed (Table 1), which is unfavorable with regard to the practical application of MCDI technology. As such, assuming that the effluent sulfate concentration is maintained below the threshold of 300 mg L^{-1}, it is more advantageous to adopt a smaller adsorption current and a higher pump flow rate resulting in higher water recovery and lower energy consumption.

That is to say, the favorable adsorption current and pump flow rate were 2 A and 50 mL min^{-1}, respectively. As for the effects of ending cell voltage, it was found that the steady-state effluent sulfate and chloride concentrations and the water recovery remained almost unchanged while the energy consumption decreased with decreasing ending cell voltage (Fig. 5 and Table 1), suggesting that a smaller ending cell voltage was preferred. However, it is worth noting that the ending cell voltage required a certain minimum value to ensure that the target of 300 mg L^{-1} effluent sulfate concentration could be reached. In other words, switching to higher frequency changes between the adsorption and desorption steps instead of charging the MCDI cells for a long period is most likely a better operational scheme. From Figs. 3–5, it is also interesting to observe that the adsorption current had no influence while the pump flow rate and ending cell voltage had a slight influence on the value of the relatively steady effluent sulfate and chloride concentrations during desorption when the desorption current was kept constant for source waters of particular composition. By contrast, a more negative desorption current contributed to higher effluent sulfate and chloride concentrations during desorption as displayed in Fig. 6. The effluent sulfate concentration during desorption at a desorption current of -5 A was triple that of the feed sulfate concentration, suggesting the possibility of recovery of sulfate from the concentrate stream by precipitation of valuable minerals such as gypsum. In addition, with an increase in the intensity of the desorption current, higher water recovery and energy consumption for the range of desorption currents examined were observed (Table 1), which indicates that a more negative desorption current is desirable if the electrical energy cost is not critical. To conclude, for the case of 2 A adsorption current and 50 mL min^{-1} pump flow rate, on the premise that the effluent sulfate concentration is maintained below 300 mg L^{-1}, the other two optimal operating parameters were an appropriately minimized ending cell voltage and a desorption current representing a trade-off between water recovery and energy consumption.

The above discussion is based on the combination of 2 A adsorption current and 50 mL min^{-1} pump flow rate. In fact, other combinations of adsorption current and pump flow rate could also reduce the effluent sulfate concentration to 300 mg L^{-1} for a given feed solution of 1000 mg L^{-1} sulfate and 500 mg L^{-1} chloride. For example, as shown in Figs. S5–S8, under 1 A adsorption current and 25 mL min^{-1} pump flow rate, or 4 A adsorption current and 100 mL min^{-1} pump flow rate, 300 mg L^{-1} steady-state effluent sulfate concentration was reached during adsorption and the profiles of dynamic effluent sulfate and chloride concentrations in the whole cycle at different ending cell voltages and desorption current behaved similarly to those under 2 A adsorption current and 50 mL min^{-1} pump flow rate. Here, we introduce another indicator to characterize the differential adsorption between sulfate and chloride, i.e., sorption ratio of sulfate to chloride, which refers to the ratio of sulfate adsorption to chloride adsorption per cycle. Fig. 7 shows the optimization mapping of water recovery-energy consumption and sorption ratio of sulfate to chloride-energy consumption as a function of ending cell voltage and desorption current under the three examined combinations of adsorption current and pump flow rate with experimental data closer to the top left corner considered to be more preferable. It can be seen from Fig. 7a that, among these three combinations, the combination of 1 A adsorption current and 25 mL min^{-1} pump flow rate resulted in the highest water recovery and lowest energy consumption, implying that a smaller adsorption current and a lower matching pump flow rate could be more favorable in practical applications. Similar trends in water recovery and energy consumption with increasing ending cell voltage or desorption current were observed for all the three combinations, i.e., increasing the ending cell
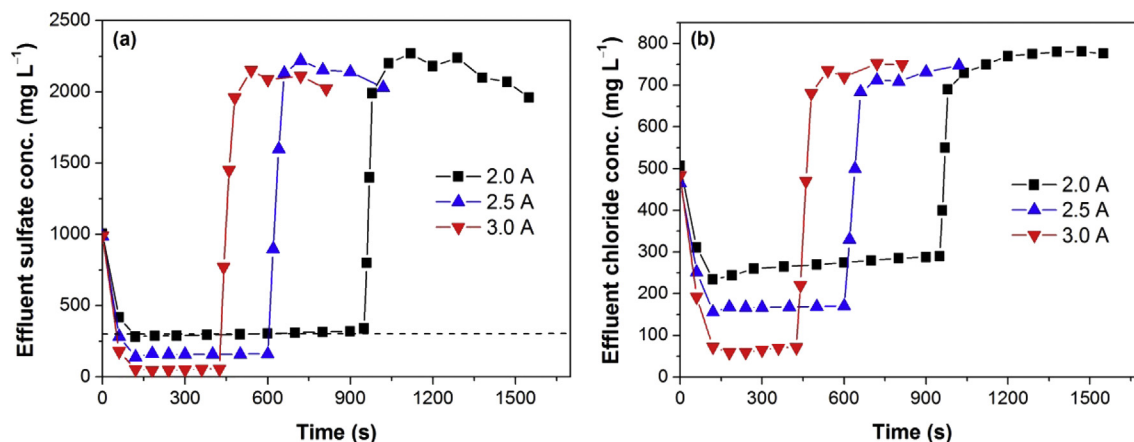
Fig. 3. Effects of adsorption current on the effluent (a) sulfate and (b) chloride concentrations on the premise of maintaining the effluent sulfate concentration below 300 mg L^{-1}. Experimental conditions: sulfate feed concentration 1000 mg L^{-1}, chloride feed concentration 500 mg L^{-1}, pump flow rate 50 mL min^{-1}, ending cell voltage 1.5 V and desorption current −3 A.
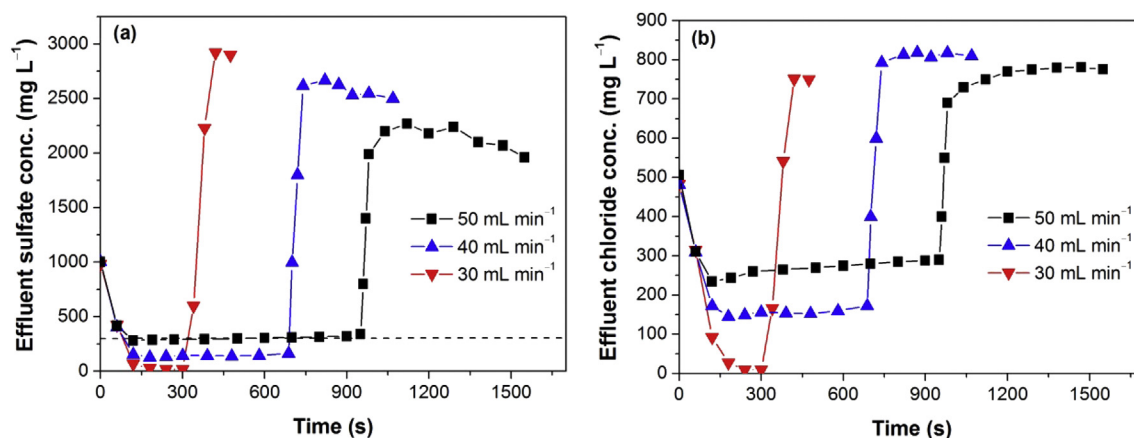

Fig. 4. Effects of pump flow rate on the effluent (a) sulfate and (b) chloride concentrations on the premise of maintaining the effluent sulfate concentration below 300 mg L^{-1}. Experimental conditions: sulfate feed concentration 1000 mg L^{-1}, chloride feed concentration 500 mg L^{-1}, adsorption current 2 A, ending cell voltage 1.5 V and desorption current −3 A.

voltage led to stable water recovery and higher energy consumption while increasing the intensity of desorption current led to both higher water recovery and energy consumption. Likewise, in Fig. 7b, the combination of a smaller adsorption current and the lower matching pump flow rate contributed favorably to larger sorption ratio of sulfate to chloride (i.e., larger preferential adsorption of sulfate over chloride as the sulfate and chloride feed concentrations were both fixed) and lower energy consumption. Meanwhile, it can be known from Fig. 7b that an increase in the ending cell voltage led to a slightly smaller preferential adsorption of sulfate over chloride while the desorption current had no impact. It should be noted that, here, the reason why the sorption ratio of sulfate to chloride was only slightly above 1 is due to the lower feed molar concentration of sulfate (10.4 mM) than chloride (14.1 mM), rather than the weak preferential adsorption of sulfate over chloride in MCDI cells. Fig. 8 shows the linear positive correlation between the sorption ratio of sulfate to chloride and the feed molar concentration ratio of sulfate to chloride. If no preferential adsorption exists between sulfate and chloride, the sorption ratio of sulfate to chloride would increase in direct proportion to the feed molar concentration ratio of sulfate to chloride according to $y = x$. The experimental results indicate a slope for the sorption ratio of sulfate to chloride as a function of feed molarity ratio of 1.58

indicating that preferential adsorption of sulfate over chloride occurred. In other words, 36.7% (0.58/1.58) of the adsorbed sulfate may be attributed to the preferential adsorption of sulfate over chloride.

As suggested above, the preferential adsorption of sulfate over chloride by MCDI may be enhanced to some degree by appropriately adjusting the operating parameters (e.g., a smaller adsorption current and a lower matching pump flow rate) when the sulfate and chloride feed concentrations are both fixed. Nevertheless, the improved value is still considered small compared to nanofiltration (NF). NF is an effective pressure-driven membrane process with membrane pore size, operation pressure and cut-off ability between that of ultrafiltration and reverse osmosis (Zhou et al., 2015). Important features of NF membranes include low rejection of monovalent ions, high retention of divalent/multivalent ions and organic molecules above molecular weight of 300 (Lu et al., 2002; Mohammad et al., 2015). It has been reported that, for mixed salt solutions (NaCl and Na$_2$SO$_4$), sulfate can be almost totally retained by NF membranes while rejection to chloride is low and, in some instances, negative rejection to chloride might occur (Luo and Wan, 2013; Tanninen et al., 2006). These properties may suggest that NF is a better choice than MCDI in treatment of brackish waters containing excessive sulfate. However, in fact, complete or near

Table 1
Water recovery and energy consumption for single-pass constant-current MCDI under reverse-current desorption on the premise of maintaining the effluent sulfate concentration below 300 mg L^{-1} for a given feed solution of 1000 mg L^{-1} sulfate and 500 mg L^{-1} chloride, as a function of operating parameters varied around the reference settings: adsorption current 2 A, pump flow rate 50 mL min^{-1}, ending cell voltage 1.5 V and desorption current −3 A.

Operating parameters	Water recovery	Energy consumption (kJ m^{-3})
Adsorption current: pump flow rate 50 mL min^{-1}, ending cell voltage 1.5 V, desorption current −3 A		
2.0 A	64%	3206
2.5 A	59%	4409
3.0 A	52%	5286
Pump flow rate: adsorption current 2 A, ending cell voltage 1.5 V, desorption current −3 A		
30 mL min^{-1}	62%	5690
40 mL min^{-1}	63%	4182
50 mL min^{-1}	64%	3206
Ending cell voltage: adsorption current 2 A, pump flow rate 50 mL min^{-1}, desorption current −3 A		
0.6 V	66%	2200
0.9 V	65%	2529
1.2 V	64%	2782
1.5 V	64%	3206
Desorption current: adsorption current 2 A, pump flow rate 50 mL min^{-1}, ending cell voltage 1.5 V		
−2 A	53%	3014
−3 A	64%	3206
−4 A	70%	3576
−5 A	76%	3752

complete removal of sulfate is unnecessary in most instances. After all, sulfate is not toxic and the maximum permissible sulfate concentration can be as high as several hundred milligrams per litre. Recognizing this, we see (M)CDI as a promising alternative method for both sulfate and chloride removal with the results of this study contributing to both fundamental understanding of the (M)CDI separation process and insight into operating conditions suited to achieving suitable treated water quality (rather than complete ion fractionation) for a particular energy input. Admittedly, when (M) CDI is applied to treat brackish waters containing high levels of toxic ions such as arsenate, chromate and fluoride, certain improvements should be made to increase the extent of preferential ion adsorption, e.g., coating the carbon electrode surface with an anion-exchange resin powder with high affinity toward the contaminant ion of concern (Kim and Choi, 2012), since the maximum permissible concentrations of these ions in treated waters are low.

4. Conclusions

The field of CDI has progressed enormously in the past decade and is currently being actively explored for water treatment including brackish water desalination and wastewater remediation. In this study, the feasibility of sulfate removal from brackish water by single-pass constant-current MCDI under reverse-current desorption has been investigated. Compared to chloride, sulfate
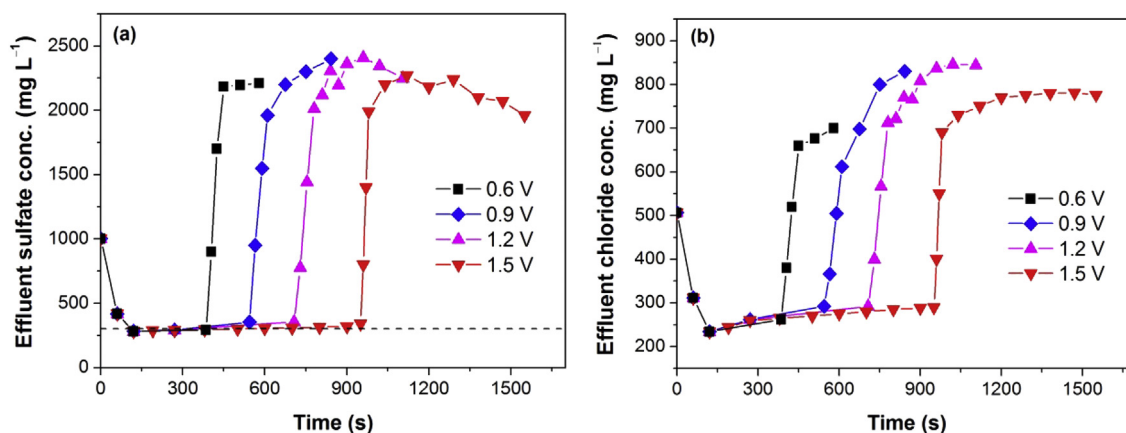

Fig. 5. Effects of ending cell voltage on the effluent (a) sulfate and (b) chloride concentrations. Experimental conditions: sulfate feed concentration 1000 mg L^{-1}, chloride feed concentration 500 mg L^{-1}, adsorption current 2 A, pump flow rate 50 mL min^{-1} and desorption current −3 A.
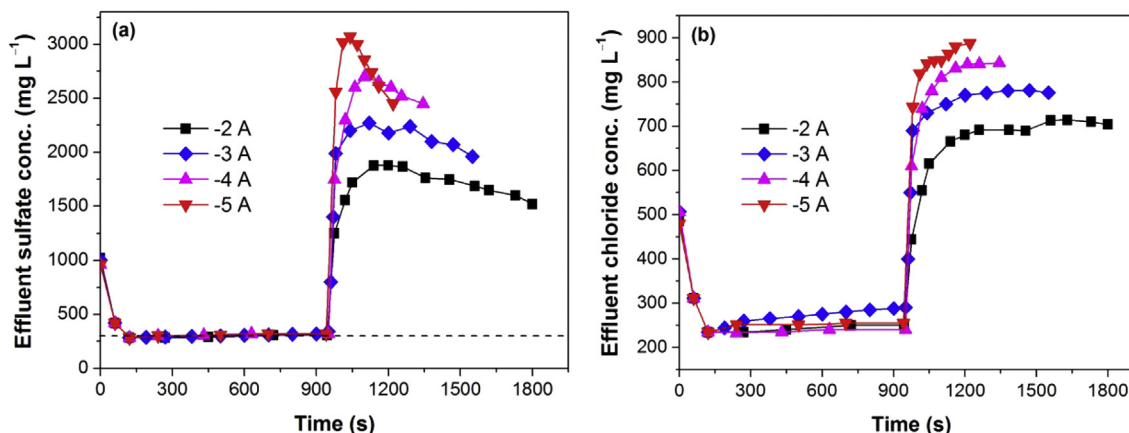

Fig. 6. Effects of desorption current on the effluent (a) sulfate and (b) chloride concentrations. Experimental conditions: sulfate feed concentration 1000 mg L^{-1}, chloride feed concentration 500 mg L^{-1}, adsorption current 2 A, pump flow rate 50 mL min^{-1} and ending cell voltage 1.5 V.
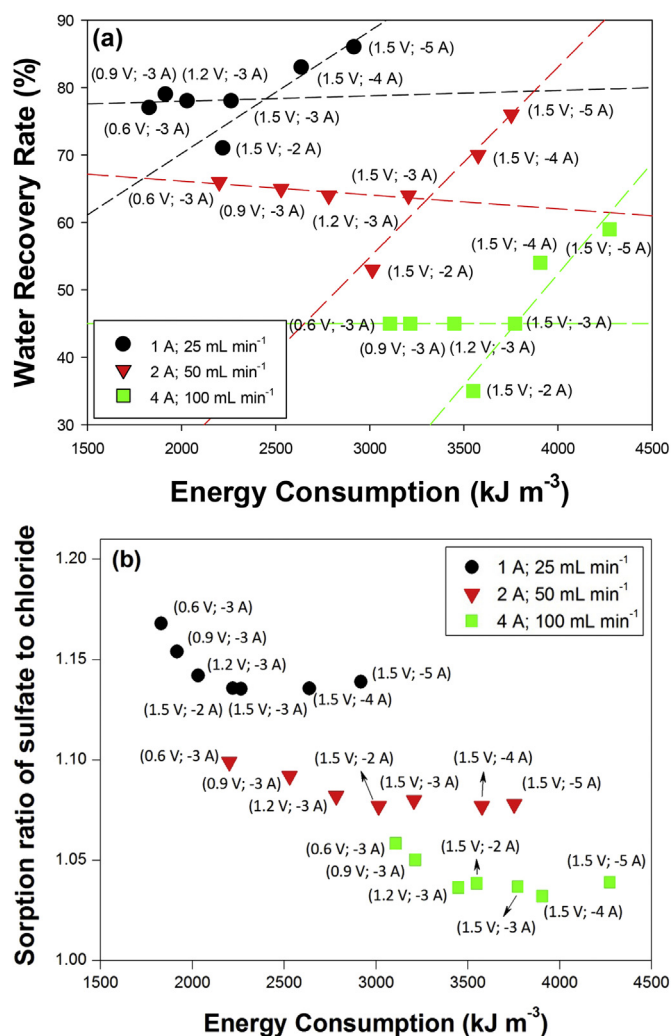
Fig. 7. Optimization maps of water recovery-energy consumption and sorption ratio of sulfate to chloride-energy consumption. All the three combinations of adsorption current and pump flow rate (1 A, 25 mL min^{-1}; 2 A, 50 mL min^{-1}; 4 A, 100 mL min^{-1}) could reduce the effluent sulfate concentration to 300 mg L^{-1} for a given feed solution of 1000 mg L^{-1} sulfate and 500 mg L^{-1} chloride.

Fig. 8. Relationship between sorption ratio of sulfate to chloride and feed molarity ratio of sulfate to chloride. Experimental conditions: adsorption current 2 A, desorption current −3 A, pump flow rate 50 mL min^{-1} and ending cell voltage 1.2 V; The total feed molarity of sulfate and chloride is 30 mM.

was preferentially removed from the bulk solution within the spacer channel of MCDI cells. We systematically varied four input operating parameters, namely, adsorption current, pump flow rate, ending cell voltage and desorption current, and examined their effects on three performance indicators (i.e., water recovery, energy consumption and sorption ratio of sulfate to chloride) on the premise that the effluent sulfate concentration was maintained below the specified threshold of 300 mg L^{-1}. The procedure for optimization of the four operating parameters has been presented with results indicating that the combination of a smaller adsorption current and a lower matching pump flow rate was more preferable as they led to higher water recovery, larger preferential adsorption of sulfate over chloride and lower energy consumption. The favoured ending cell voltage was an appropriately minimized value while the preferred desorption current represented a trade-off between water recovery and energy consumption. As the scale-up of MCDI is readily achieved through increase in the number of electrode pairs in MCDI cells and/or the establishment of parallel MCDI modules, the findings obtained in this study should contribute to the optimization of operating conditions when scaled up MCDI is applied to treatment o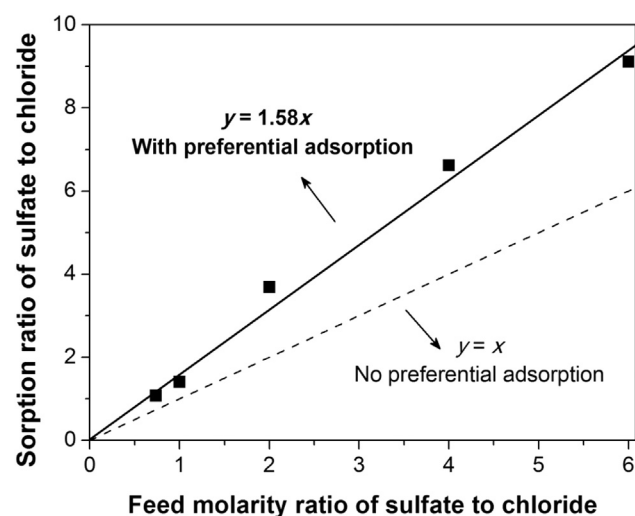f real waters containing dual or even multiple anions on the condition that the concentration of one anion (such as sulfate) is excessive and the effluent concentration of this anion needs to be maintained below a specified threshold. Such analyses are considered indispensable to the economic and sustainable implementation of MCDI technology in water treatment.

Acknowledgements

Appendix A. Supplementary data

Supplementary data related to this article can be found at http://dx.doi.org/10.1016/j.watres.2017.05.046.

References

Bian, Y., Yang, X., Liang, P., Jiang, Y., Zhang, C., Huang, X., 2015. Enhanced desalination performance of membrane capacitive deionization cells by packing the flow chamber with granular activated carbon. Water Res. 85, 371–376.
Biesheuvel, P.M., Zhao, R., Porada, S., van der Wal, A., 2011. Theory of membrane capacitive deionization including the effect of the electrode pore space. J. Colloid Interface Sci. 360 (1), 239–248.
Călinescu, O., Marin, N.M., Ioniţă, D., Pascu, L.F., Tudorache, A., Surpăţeanue, G., Badea, I.A., Aboul-Enein, H.Y., 2016. Selective removal of sulfate ion from different drinking waters. Environ. Nanotechnol. Monit. Manag. 6, 164–168.
Chen, Y., Wen, Y., Zhou, Q., Huang, J., Vymazal, J., Kuschk, P., 2016. Sulfate removal and sulfur transformation in constructed wetlands: the roles of filling material and plant biomass. Water Res. 102, 572–581.
Choi, J.H., 2014. Determination of the electrode potential causing Faradaic reactions in membrane capacitive deionization. Desalination 347, 224–229.
Cohen, I., Avraham, E., Bouhadana, Y., Soffer, A., Aurbach, D., 2015. The effect of the flow-regime, reversal of polarization, and oxygen on the long term stability in capacitive de-ionization processes. Electrochim. Acta 153, 106–114.
Crow, D.R., 1994. Principles and Applications of Electrochemistry, fourth ed. Blackie Academic & Professional, London.
Dykstra, J.E., Zhao, R., Biesheuvel, P.M., van der Wal, A., 2016. Resistance identification and rational process design in capacitive deionization. Water Res. 88, 358–370.

Flury, M., Gimmi, T., 2002. Solute diffusion. In: Dane, J.H., Topp, G.C. (Eds.), Methods of Soil Analysis, Part 4, Physical Methods. Soil Science Society of America, Madison, WI, pp. 1323–1351.

Gao, X., Omosebi, A., Landon, J., Liu, K., 2015a. Enhanced salt removal in an inverted capacitive deionization cell using amine modified microporous carbon cathodes. Environ. Sci. Technol. 49 (18), 10920–10926.

Gao, X., Omosebi, A., Landon, J., Liu, K., 2015b. Surface charge enhanced carbon electrodes for stable and efficient capacitive deionization using inverted adsorption–desorption behavior. Energy Environ. Sci. 8, 897–909.

Garcia-Quismondo, E., Santos, C., Soria, J., Palma, J., Anderson, M.A., 2016. New operational modes to increase energy efficiency in capacitive deionization systems. Environ. Sci. Technol. 50 (11), 6053–6060.

Guimarães, D., Leão, V.A., 2014. Batch and fixed-bed assessment of sulphate removal by the weak base ion exchange resin Amberlyst A21. J. Hazard. Mater. 280, 209–215.

Huyskens, C., Helsen, J., de Haan, A.B., 2013. Capacitive deionization for water treatment: screening of key performance parameters and comparison of performance for different ions. Desalination 328, 8–16.

Kang, J., Kim, T., Shin, H., Lee, J., Ha, J.I., Yoon, J., 2016. Direct energy recovery system for membrane capacitive deionization. Desalination 398, 144–150.

Kim, Y.J., Choi, J.H., 2012. Selective removal of nitrate ion using a novel composite carbon electrode in capacitive deionization. Water Res. 46, 6033–6039.

Lu, X., Bian, X., Shi, L., 2002. Preparation and characterization of NF composite membrane. J. Membr. Sci. 210 (1), 3–11.

Luo, J., Wan, Y., 2013. Effects of pH and salt on nanofiltration—a critical review. J. Membr. Sci. 438, 18–28.

Mohammad, A.W., Teow, Y.H., Ang, W.L., Chung, Y.T., Oatley-Radcliffe, D.L., Hilal, N., 2015. Nanofiltration membranes review: recent advances and future prospects. Desalination 356, 226–254.

Mossad, M., Zou, L., 2012. A study of the capacitive deionisation performance under various operational conditions. J. Hazard. Mater. 213–214, 491–497.

Mossad, M., Zou, L., 2013. Study of fouling and scaling in capacitive deionisation by using dissolved organic and inorganic salts. J. Hazard. Mater. 244–245, 387–393.

Porada, S., Zhao, R., van der Wal, A., Presser, V., Biesheuvel, P.M., 2013. Review on the science and technology of water desalination by capacitive deionization. Prog. Mater. Sci. 58 (8), 1388–1442.

Qu, Y., Baumann, T.F., Santiago, J.G., Stadermann, M., 2015. Characterization of resistances of a capacitive deionization system. Environ. Sci. Technol. 49, 9699–9706.

Runtti, H., Luukkonen, T., Niskanen, M., Tuomikoski, S., Kangas, T., Tynjälä, P., Tolonen, E., Sarkkinen, M., Kemppainen, K., Rämö, J., Lassi, U., 2016. Sulphate removal over barium-modified blast-furnace-slag geopolymer. J. Hazard. Mater. 317, 373–384.

Silva, A.M., Lima, R.M.F., Leão, V.A., 2012. Mine water treatment with limestone for sulfate removal. J. Hazard. Mater. 221–222, 45–55.

Suss, M.E., Porada, S., Sun, X., Biesheuvel, P.M., Yoon, J., Presser, V., 2015. Water desalination via capacitive deionization: what is it and what can we expect from it? Energy Environ. Sci. 8, 2296–2319.

Tang, W., Kovalsky, P., He, D., Waite, T.D., 2015. Fluoride and nitrate removal from brackish groundwaters by batch-mode capacitive deionization. Water Res. 84, 342–349.

Tang, W., Kovalsky, P., Cao, B., He, D., Waite, T.D., 2016. Fluoride removal from brackish groundwaters by constant current capacitive deionization (CDI). Environ. Sci. Technol. 50 (19), 10570–10579.

Tanninen, J., Mänttäri, M., Nyström, M., 2006. Effect of salt mixture concentration on fractionation with NF membranes. J. Membr. Sci. 283, 57–64.

Zhao, R., Satpradit, O., Rijnaarts, H.H.M., Biesheuvel, P.M., van der Wal, A., 2013. Optimization of salt adsorption rate in membrane capacitive deionization. Water Res. 47 (5), 1941–1952.

Zhou, D., Zhu, L., Fu, Y., Zhu, M., Xue, L., 2015. Development of lower cost seawater desalination processes using nanofiltration technologies — A review. Desalination 376, 109–116.